

# Active fault segmentation in southwest Bulgaria and Coulomb stress triggering of the 1904 earthquake sequence

Ganas Athanassios<sup>a,\*</sup>, Shanov Stefan<sup>b</sup>, Drakatos George<sup>a</sup>, Dobrev Nikolai<sup>b</sup>, Sboras Sotiris<sup>c</sup>, Tsimi Christina<sup>a</sup>, Frangov Georgi<sup>b</sup>, Pavlides Spyros<sup>c</sup>

<sup>a</sup> National Observatory of Athens, Institute of Geodynamics, P.O. Box 20048, Lofos Nymfon, Thission, Athens 11810, Greece

<sup>b</sup> Bulgarian Academy of Sciences, Geological Institute, Acad. G. Bonchev Str., Buil. 24, 1113 Sofia, Bulgaria

<sup>c</sup> Aristotle University of Thessaloniki, Department of Geology, Thessaloniki 54124, Greece

Received 20 September 2004; received in revised form 31 March 2005; accepted 18 July 2005

## Abstract

We combined field mapping and structural analysis of Landsat imagery in order to identify active faults in the broader area of the Simitli graben and to the east towards the cities of Razlog and Bansko, in southwest Bulgaria. We mapped five large active fault segments with normal-slip kinematics and down-to-north displacement and three smaller, antithetic faults near Razlog. Our work suggests that: (a) present-day deformation in SW Bulgaria is extensional and is accommodated by seismic slip along E–W, NE–SW and WN–ESE normal faults; (b) inversion of fault slip data shows a  $\sigma_3$  axis oriented  $336\text{--}356^\circ$ ; (c) the Krupnik fault comprises one earthquake segment with a general NE–SW strike and dip to the N–NW; its length is about 20 km so its earthquake potential is of the order of  $M_w = 6.7 \pm 0.3$ ; (d) as the 4 April, 1904 earthquake comprised two events, a static stress triggering hypothesis may apply, which is also compatible with the fault segmentation, geomorphology and the macroseismic reports. Source faults for the first event (10:02 a.m.) may have been either the 12 km long Gradevo fault or the 11 km long Elovitsa fault. We estimate a moment magnitude of 6.3 for this event. The first event triggered the second one (10:28 a.m.) on the Krupnik fault.

© 2005 Elsevier Ltd. All rights reserved.

**Keywords:** Active faults; Stress transfer; Fault geometry; Slip rate; Bulgaria; Krupnik

## 1. Introduction

Southwest Bulgaria has a high seismicity record and a history of strong earthquakes. For example, the two earthquakes in 4 April, 1904 inside the Struma valley are among the largest, shallow 20th century events on land in the Balkans (Ambraseys and Jackson, 1998). The two shocks devastated the region of the Struma valley down to the town of Sandanski with major damage affecting the towns of Krupnik, Razlog and many smaller villages (Fig. 1). The main shock occurred at 10:25 a.m. (GMT; Shebalin et al., 1974) and it was preceded by a large foreshock (10:02 a.m.). The foreshock occurred in the area to the northeast of the mainshock (Shebalin et al., 1974; Meyer et al., 2002). After the 1904 events the Krupnik–Simitli area continued to show high seismicity rates (Dineva et al., 1998), which indicates both a significant degree of strain localization and fast recovery of the stress field levels. A strong earthquake also occurred in 1964 near the city of Razlog (Fig. 1; Grigorova et al., 1966). The latter event suggested the occurrence of more active

\* Corresponding author.

E-mail address: [aganas@gein.noa.gr](mailto:aganas@gein.noa.gr) (G. Athanassios).

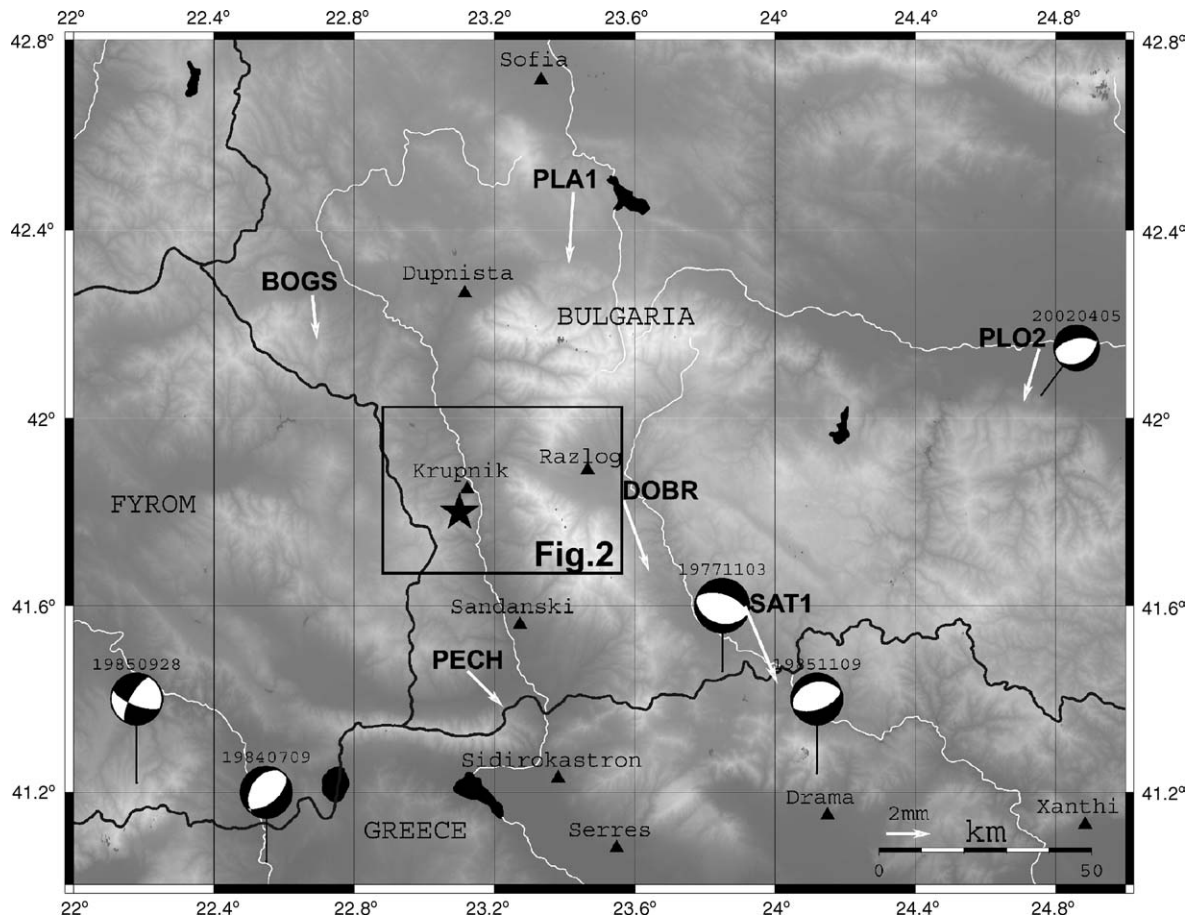


Fig. 1. Elevation map of south Bulgaria, FYROM and northern Greece showing focal mechanisms of most important events since 1977. Gray levels correspond to land elevations: dark: low, bright: high. Focal mechanism data come from the Harvard CMT catalogue and the MEDNET RCMT catalogue (see Table 1 for details). GPS vectors (white arrows) are after Kotzev et al. (2001). Both focal mechanism data and GPS velocities indicate that regional strain is predominantly N–S ( $\pm 20^\circ$ ) extension throughout this area. The black star indicates the 1904 earthquake epicentre according to Ambraseys and Jackson (1998). Rectangular box indicates the study area.

faults in this region which motivated our study. In addition, Bulgarian researchers in association with Czech engineers have been monitoring motions along several faults in the study area by means of TM-71 extensometers (Dobrev and Kostak, 2000; Dobrev et al., 2004). The instrument on the Krupnik fault has recorded an average left-lateral motion of the two blocks of 2.7 mm/a along with a shortening component of 1.9 mm/a. The measurements span a period of 17 years. Van Eck and Stoyanov (1996) modeled seismic hazard in southwest Bulgaria and they found with 50% confidence that this area shows 1% annual probability to exceed 0.3 g. In addition, Tsapanos et al. (2002) examined the probability for a magnitude 7.0 event during a time period of 100 years for a large sector of central

Table 1  
Parameters of earthquakes shown in Fig. 1

Date	Time (GMT)	Epicentre	$M_w$	Fault plane (strike/dip/rake)
3 November 1977	02:22:57.1	41.46, 23.85	5.5	104/35/–94
9 July 1984	18:57:14.7	41.05, 22.55	5.2	212/38/–105
28 September 1985	14:50:20.0	41.22, 22.18	5.2	209/70/–158
9 November 1985	23:30:47.7	41.24, 24.12	5.2	256/33/–85
5 April 2002	13:14:02.9	42.05, 24.76	4.6	059/35/–106

Events from 1977 to 1985 are from the Harvard On-line Catalogue. The 2002 event is from the RCMT On-line Catalogue.

Balkans including the study area of Fig. 1. They concluded that this area has the largest probability with a value of 0.306.

According to the old instrumental data the earthquake magnitudes ranged between 7.1 and 7.3 for the first shock and 7.7–7.8 for the second one (Christoskov and Grigorova, 1968; Shebalin et al., 1974). Similar magnitude values for the two events, 7.2 and 7.8, respectively, were calculated by the maximum accelerations reconstructed by Rangelov and Paskaleva (1998). The spectrum of secondary effects also supports  $M > 7.5$  for the main shock (Rangelov et al., 2000, 2001), which corresponds to  $M = 7.5$  given by Gutenberg and Richter (1954). However, Ambraseys (2001) reappraised the instrumental data proposing a value of  $M_s = 7.2$ , while his re-assessment of the intensity distribution suggests 7.1. Rangelov et al. (2000) suggested a magnitude range of 6.5–6.7 for both events on the basis of neotectonics, extreme value method, recurrence graph and geodetic data. Dineva et al. (2002) re-determined the 1904 earthquake magnitudes as  $M_w = 6.8$  and  $M_s = 7.2$ , respectively. Recently, Meyer et al. (2002) using satellite imagery and field observations, mapped 20–35 km long active faults close to, or within, the 1904 epicentral area. These authors suggest that faulting was initiated during Miocene times (13 Ma) and estimated the long-term slip-rate to be 0.15 mm/a on the Krupnik fault. A possible rupture of the Krupnik fault compatible with their observations would account for a magnitude  $M_s = 6.9$ .

Thus, the majority of the recent studies in this region suggest a downsizing of earthquake magnitudes for the 1904 sequence. New estimates of earthquake magnitudes may also result if we consider the 1904 sequence as two independent events whose effects were combined to produce the devastating effect described in literature. This is a possible scenario that has not been examined so far. Such a hypothesis may involve reactivation of two neighbouring but different faults or fault segments of the same fault zone because of Coulomb stress transfer (e.g., King et al., 1994). This view is enhanced by the geological findings of this work and is elaborated further below.

First, we investigated the segmentation pattern in the region of the 1904 events. The geological map of the area (Marinova and Zagorchev, 1993; Dobrev, 1999) shows large, normal faults separating Neogene sedimentary rocks from igneous and metamorphic basement (Fig. 2). A tentative interpretation may be that active faulting during Neogene time has resulted in the formation of two elongated basins and the emergence of the Pirin mountain range (Fig. 2). The basins are oriented E–W to WSW–ENE (Simitli) and WNW–ESE (Razlog; Fig. 2; Zagorchev, 1992). Both basins

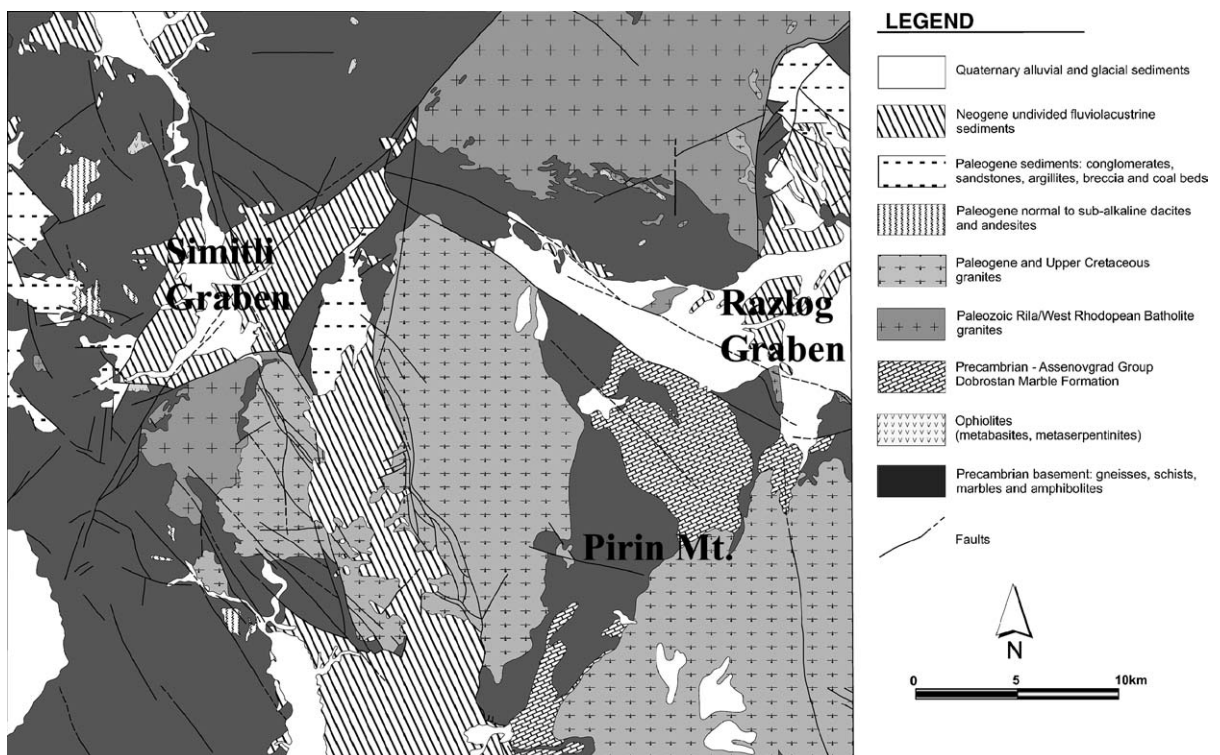


Fig. 2. Simplified geological map of the study area (modified after Marinova and Zagorchev, 1993).

are filled by Neogene sedimentary rocks such as sandstones, conglomerates, clays and coal. The maximum Neogene thickness is about 1500 m in the central sector of the Simitli graben (Dobrev, 1999). The surrounding mountains Pirin (South) and Rila (North) are formed by metamorphic and magmatic rocks comprising amphibolites, gneisses, marbles and granites. Our approach comprises use of satellite imagery to identify normal faults (e.g., Ganas et al., 2001, 2004) followed by geomorphologic observations on drainage and faceted spurs patterns and structural measurements in the field. After establishing the fault pattern, we apply fault-slip models to stress transfer scenarios. Our modeling indicates a possible triggering mechanism for the 1904 sequence.

## 2. The geometry of active faults and footwall geomorphology

### 2.1. Landsat interpretation

We selected a Landsat 5 scene of the path/row 184/31 reference frame. This scene is particularly suited for structural interpretations because of the low-sun angle ( $47^\circ$ ) during its acquisition date (2 September, 1992) and its geometric rectification into the UTM projection that allows for on-screen measurements of distances and angles. The low sun-angle combined with a southeastern sun azimuth ( $N134^\circ E$ ) in the image selected, provide an almost ideal imaging geometry for E–W ( $\pm 20^\circ$ ) striking normal faults, downthrowing to the north, such as the Krupnik fault segment (Fig. 3). This is because relief created by the dome-shaped footwall uplift along isolated normal fault segments casts long shadows to the north of the faults (e.g., Ganas and White, 1996; Ganas, 2002). Shadow widths will diminish towards segment boundaries because of decreasing relief. For example, in central Greece normal fault segments terminate in regions of (i) low topography and (ii) minimum footwall “hinterland” development (e.g., Roberts and Koukouvelas, 1996; Ganas et al., 2001, 2004).

In Fig. 3, several E–W lineaments across the image are large, normal faults. The lineaments are of morphologic origin (a directional break in surface slope) and of low sinuosity as expected for active faults where earthquake recurrence rates keep pace with erosion rates. Notice that structural and geomorphic features predicted by segmentation theory (e.g., Crone and Haller, 1991) to occur at the ends of active faults also are clear on this image (Fig. 3). These include (1) transverse bedrock ridges at both ends of Krupnik fault and (2) the large, left-step between the Predela and Dobrinishte faults. Also, footwall drainage occurs in the form of “wine-glass” valleys; such features are known to characterise the central portions of normal fault segments (Wallace, 1978). In Fig. 4, it can be seen that drainage associated with the

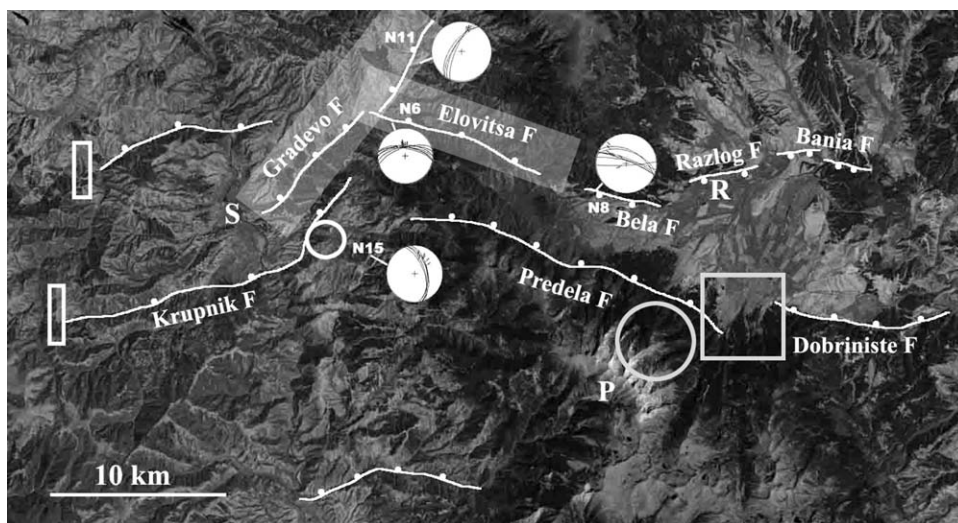


Fig. 3. Landsat TM satellite image of the study area showing active faults with ticks on the downthrown side. Letters S, R indicate Simitli graben and Razlog graben, respectively. Letter P indicates position of Pirin Mountain peak. Landsat data shown are band 5 (near infrared) taken on 2 September, 1992 (path 184, row 31). Circles represent plots of equal-area, lower hemisphere projections of fault planes and slip vectors. Large gray box indicates left step along the Predela fault. Small gray boxes indicate transverse bedrock ridges. Open circles indicate “wine-glass” valleys. Highlighted rectangles indicate modeled source faults for the first event of the 1904 sequence.

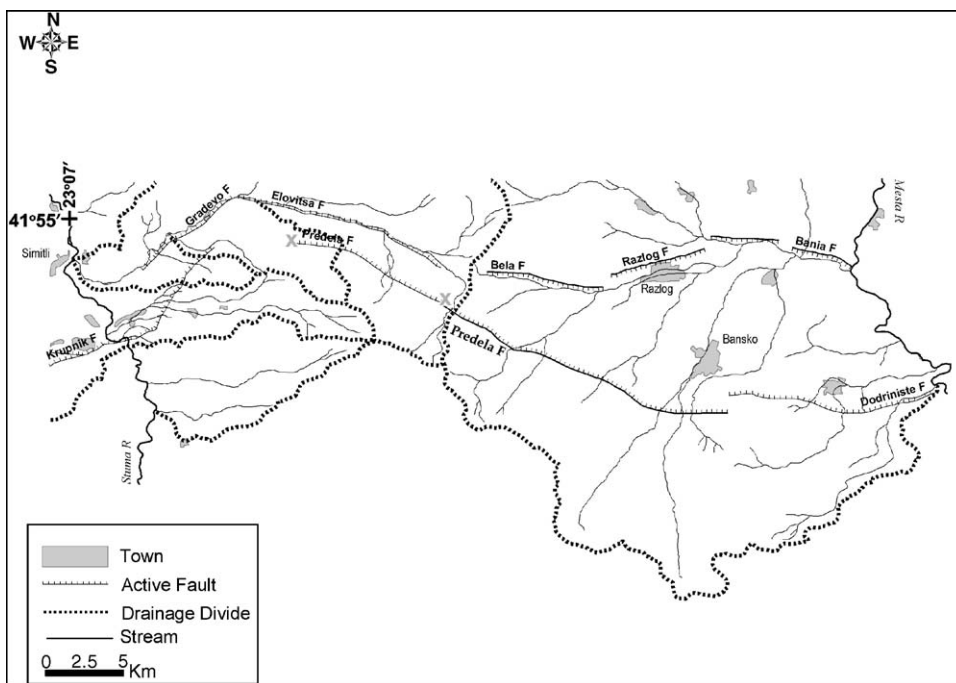


Fig. 4. Map of the study area showing main geomorphic features. Active faults are shown in black with ticks on the downthrown side. X symbols indicate inactive segment along the Predela fault. All rivers and streams are shown as thin black lines. Large catchments are shown as dotted lines. Gray polygons depict towns and villages. Stream flows are controlled by the active basin depocentres in the regions of Krupnik (west) and Razlog (east).

wine-glass valleys along the Predela Fault is directed north–south whereas hangingwall drainage is flowing to the East (river Mesta) and to the west (river Struma), respectively.

Further observations on the tectonic geomorphology of the region show that the Pirin Mountain is elongated, with a central drainage divide running roughly along the long axis of the range (Fig. 4). The major catchments that drain the range trend nearly normal to this central crest and are separated by a set of spurs or ridges (Fig. 4). Draped over this framework are a number of distinctive landforms such as triangular facets, wine-glass canyons and regularly spaced catchments (Fig. 4). On the active hangingwall lies the piedmont area, whose origin is linked to that of the Pirin itself. The piedmont consists of a set of alluvial or debris-flow fans, possibly coalesced to form a bajada.

In summary, there are three pieces of information provided by the structural and geomorphological interpretation of Figs. 3 and 4: (a) the systematic decay of rectilinear, footwall valleys (“wine-glass”) towards both ends of lineaments; (b) breaks in lineament continuity suggesting fault stepping and/or locations of segment boundaries; (c) the recognition of transverse bedrock ridges at ends of lineaments. It is proposed that this arrangement of structural and geomorphic features defines the length and position of the active faults bounding the Pirin Mountain.

## 2.2. Field mapping in Simitli graben

The western part of the study area is dominated by the Simitli graben (Fig. 2), a Neogene structure about 8–10 km wide (E–W) and 7–8 km long (N–S). In this area we mapped two active faults, namely the Krupnik and Gradevo faults, both striking NE–SW and dipping to the North–Northwest (Fig. 3). Field evidence for recent activity is provided by the existence of smooth, fresh fault planes bearing slickensides. The Gradevo fault segment overlaps the Krupnik fault by about 30% and it is spaced only 4 km away from the Krupnik fault. Fault slip data from one locality near the northern part of the Gradevo segment are shown in Fig. 3 (Station N11). The Gradevo Fault is 12 km long and is broken into two segments with almost equal lengths because of the intersection with Elovitsa Fault, a more eastern fault segment (Fig. 3). Gradevo and Elovitsa Faults intersect at almost right angles and the latter structure seems to be a bit younger as it displaces the former to the right (east). Despite this fault pattern we think both faults are active and

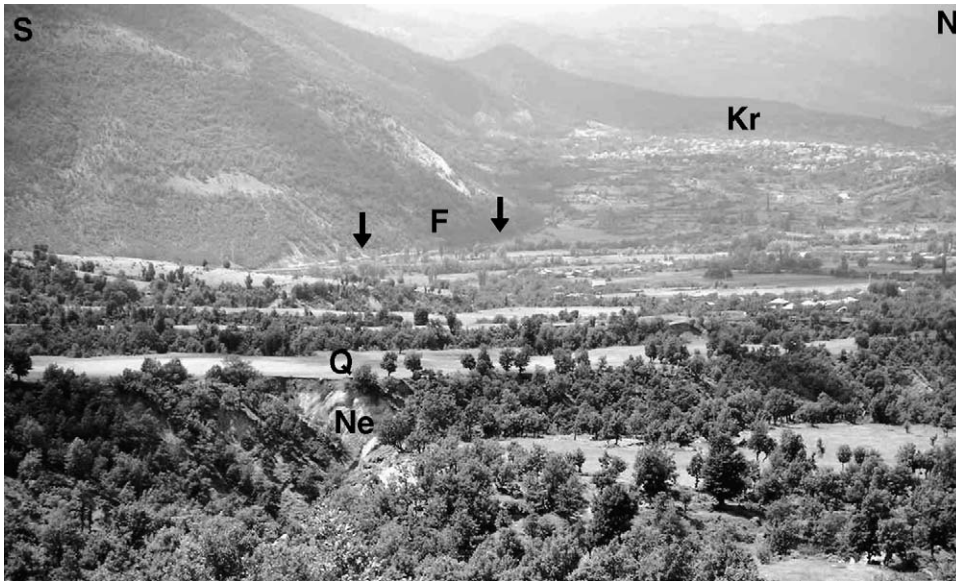


Fig. 5. Field photograph of the Simitli graben. View to the west. The Struma River flows from right to left. Highest elevation on the mountain to the left is 1138 m. The village of Krupnik is indicated by Kr. Letters Q and Ne in the foreground point to synrift deposits consisting of brown, quaternary deposits of fluvial character and yellow marls of Pliocene age, respectively. These deposits are found at the hanging wall of the Krupnik fault. The latter is marked by black arrows.

are young features in the landscape because they control drainage patterns (Fig. 4). It is probable that both faults were created after sufficient strain had been accommodated along the most “interior” normal faults of Krupnik and Predela. Two more normal faults also occur on either side of Simitli Graben in synthetic arrangement to the Krupnik fault (Fig. 3).

The mountain in the footwall of the Krupnik Fault shows high relief and typical tectonic geomorphology of active faulting including transverse elongated valleys, landslides, creep zones and rock falls. A panoramic view of the footwall area near the village of Krupnik is shown in Fig. 5. The Krupnik fault is 20 km long with a marked change in strike near Kresna pass (Fig. 6). Between points A–B the fault dips towards N353°E while between points B–D the average dip direction is N293°E. Despite this concave bend we suggest that the fault now forms one coherent fault segment. However, geomorphic analysis indicates that the Krupnik Fault grew by segment linkage of two smaller segments, which linked to each other about 1 km to the east of the Kresna pass (Fig. 6). The analysis comprises first the construction of a 20 m relief model of the Simitli graben, followed by computation of a slope map. Secondly, we mapped the triangular facets along the footwall of the fault. The mapping was conducted in ARC GIS by digitization of the triangular regions and calculation of the slope statistics. We extracted 28 facets with mean slope angles between 21° and 37°. The 21° slope occurs along a facet that is located to the south of a local splay of the fault near its western tip (Fig. 6). To the east of this locality the mean slope of facets is greater than 26°. We suggest that the along-strike difference in slope angle is a function of (a) local variations in footwall uplift rate and (b) algorithm error. Bedrock lithology, i.e. granite versus amphibolites (Fig. 2) does not seem to influence facet steepness. In addition, the alignment of triangular facets indicates that there were two proto-segments of the Krupnik Fault, AC and BD that linked to each other in the area of point B (Fig. 6). Fault ABD now behaves as one earthquake segment. Segment BC is now abandoned, there is no synrift present and the faceted spurs are slowly eroding. In the same figure we adopt a model for the formation of triangular facets due to footwall uplift across normal faults. Except for the formation of large alluvial fans, this model seems to apply in the Krupnik Fault area, as well. The absence of the large alluvial fans along the Krupnik Fault could be explained by the Quaternary fault slip-rate, because relatively high rates permit quick sediment discharge. This geomorphic characteristic sharply contrasts with the occurrence of large alluvial fans developed along the Predela normal fault which is discussed below (Fig. 7).

From borehole data the basin depth near Krupnik is estimated at 1500 m (N. Dobrev, personal communication; Fig. 5). This may be combined with the height of the mountain front (1138 m) in order to estimate total displacement across

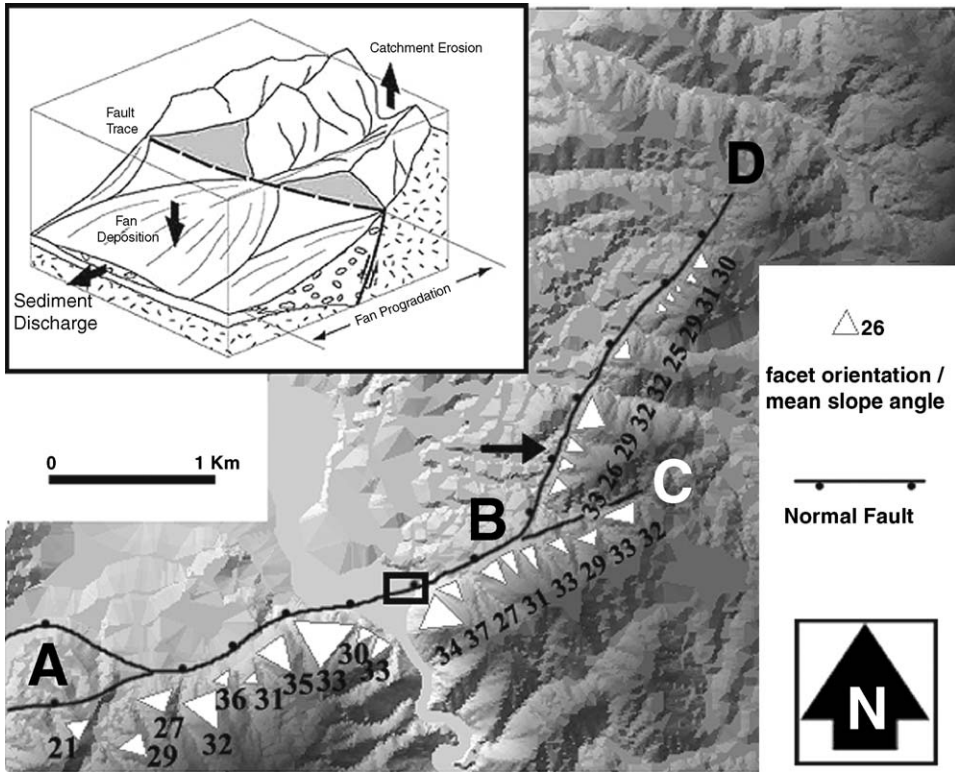


Fig. 6. Simplified neotectonic map of the mountain range front showing the trace of the Krupnik normal fault. Local shaded relief is shown in 8-bit gray levels. White triangles represent the distribution and mean slope angle of triangular facets in the footwall of the Krupnik fault. The fault is segmented into segments AC and BD. Black arrow points to locality of Fig. 9. Black rectangle shows locality of 1904 rupture where a 2 m displacement is inferred from geophysical data. Inset box shows model for facet formation after Allen and Densmore (2000).

the fault. Thus, the total throw is 2638 m. Assuming (a) pure dip-slip motion along a fault plane dipping 50–60° and (b) pre-rift flat morphology and applying simple trigonometry we obtain slip = [throw/sine (dip angle)] = 3000–3500 m. This amount of cumulative displacement suggests that the Krupnik fault may be a Neogene structure; however, it is difficult to estimate its age of initiation because of three uncertainties:



Fig. 7. Field photograph of the Predela normal fault. View to the southeast. White arrows point to the inferred location of the fault along the foothills of the Pirin mountain.

- (i) The fault-controlled Krupnik basin contains Miocene sediments, however, Miocene basins are spread out in a general NW–SE direction across South Bulgaria and North Greece (Zagorcev, 1992) and they are related to an earlier phase of extension.
- (ii) The Struma River is antecedent to the Krupnik fault because its flow is controlled by the earlier extensional phase of Middle Miocene (Badenian–Sarmatian, 16–13 Ma) times (Zagorcev, 1992).
- (iii) In the footwall of the Krupnik Fault we found only uplifted sediments of Middle Oligocene age (25–27 Ma). These rocks are coal deposits of the Goreshtitsa Formation (Vatzev, 1984) that occur in the Brezhani Area at an elevation of 630 m and a distance of 2200 m from the Fault (point N15 in Fig. 3). Clearly these sediments were deposited inside Oligocene-age grabens (Zagorcev, 1992) and were cross-cut and displaced by the younger Krupnik Fault. No younger synrift has been found.

In the area to the east of Krupnik village (Fig. 5) synrift beds of Meotian age (8–10 Ma; Zagorcev, 1992) are also tilted towards the Krupnik Fault. Assuming this age (Meotian) is the beginning age of rifting then the average slip rate of the Krupnik Fault of 0.35 mm/a. This rate differs to the one proposed by Meyer et al. (2002) by a factor of 2. Zagorcev (1992) suggests a mean rate of 0.25 mm/a for this fault.

### 2.3. Field mapping in Razlog graben

The Razlog graben is a much a wider structure 20 km to the east of the Simitli area. The graben was created by normal-slip movements along the Predela fault segment, which bounds the northern side of Pirin Mountain (Fig. 7). It is probable that total displacement along the Predela fault reaches 3.5 km similar to the Krupnik fault as footwall relief equals 2 km (Table 2). However, no outcrops of slip planes were found along the Predela fault. We extracted data on fault geometry and length by photo-interpretation from Landsat infrared imagery (Fig. 3). In addition, basin drainage is controlled by three smaller, antithetic fault segments in its hangingwall (Fig. 4). However, a synthetic normal fault segment (Elovitsa) is 11 km long and active, and controls the flow of one important tributary of Struma River. The Elovitsa fault shows several fresh fault planes bearing slickensides and a stress field analysis shows the least principal stress trending N356°E (see point N6 in Fig. 3). We suggest that this fault presently accommodates all strain in the western part of the Razlog graben so the northwestern part of the Predela fault is now inactive. Another normal fault is located to the south of the town Dobrinishte, east of the Predela segment (Fig. 3).

In the vicinity of the town of Razlog there are three active, minor normal fault segments, but their dip direction is antithetic to the Predela fault (Figs. 3 and 4). These faults are from west to east: Bela Fault (6 km long), Razlog Fault (4 km long) and Bania Fault (6.5 km long). Two of the faults (Bela and Bania) show fresh fault planes on bedrock (schist). In addition, the Bania Fault is composed of two segments with a small right-step between them (Figs. 3 and 4). The Razlog segment cuts through the graben and has a northeastern strike. Its footwall shows a dome-shape profile (Fig. 8) and is composed of Neogene marls.

On either side of the Razlog graben it is suggested that the three antithetic normal faults are the most active. Geomorphic evidence (drainage pattern; Fig. 4) indicates that present-day crustal subsidence is parallel to the strike of these segments where the streams flow to the east, towards the Mesta River (Nestos). We also note that the Razlog basin watershed is located approximately mid-way along the Predela fault (Fig. 4). This feature also suggests that the

Table 2  
Data on the geometry of the active faults in Southwest Bulgaria

Fault	Length (km)	Strike	Dip direction	Footwall relief (m)
Krupnik	20	NE–SW	NW	840
Gradevo	12	NE–SW	NW	250
Predela	12.5	WNW–ESE	NE	2000
Elovitsa	11	WNW–ESE	NE	560
Dobrinishte	11	E–W	N	2000
Bela	6	E–W	S	250
Razlog	4	ENE–WSW	S	100
Bania	6.5	E–W	S	150

For location see Figs. 3 and 4. The reported numbers for the Predela segment refer to the possibly active part of the fault.



Fig. 8. Field photograph of the Razlog normal fault. View to the Northeast. Notice the elliptical shape of the footwall profile.

western part of Predela segment is inactive and strain is accommodated by motion of the Elovitsa segment (Fig. 4). The hanging wall of Predela segment is composed of a huge quantity of alluvial fan and debris-flow deposits that are very thick (Figs. 4 and 7). The “active” Predela segment does not show evidence for fault slip comparable to that of Krupnik (0.35 mm/a). Perhaps the fault slip rate is an order of magnitude less as no fresh fault planes were mapped and hangingwall drainage is controlled by the antithetic faults (Fig. 4). In addition, large karstic springs appear at a distance of about 1.5 km from the fault line and at an elevation of 960 m indicating possible appearance of impermeable material at depth that inhibits further karstification. The karst system originates in the footwall area of the Predela fault where marble units are abundant (Fig. 2). This observation suggests that the Predela fault does not act as a barrier to karst water flow. The water movement across the fault plane also suggests that this fault is slipping with low rates during most of Quaternary time so that the karstic channels have broken into the hanging wall domain through the brecciated marble zone.

### 3. The 1904 ruptures

Field studies were also conducted to re-examine and map the 1904 ruptures. We emphasize the fact that we looked for field evidence only along the fault segments defined in Fig. 3 and not along the western prolongation of the Krupnik fault, where the 1904 contemporary reports suggest surface rupturing. At the localities we visited we found that the surface break was not preserved locally even though the footwall comprises a resistant bedrock lithology (Fig. 9; amphibolites and granodiorite). It is possible that remnants of the 1904 surface breaks still exist at remote, forested areas along the fault line in Fig. 3 and further investigations may be necessary to map them. It is also possible that segments of the rupture noted in historical records were inside the syn-rift deposits, and have since been obliterated due to man-made changes in surface morphology. However, there is no convincing evidence that surface breaks have crossed over the segment boundaries that we propose, so it seems reasonable to suggest that they have ruptured the full length of the Gradevo (or Elovitsa) and Krupnik segments, that is, for 31–32 km (Fig. 3).

In addition, our field data are insufficient to establish the dimensions, attitude and amount of dislocation, except in the vicinity of Krupnik where a diversion of the Struma River was recorded (Fig. 6). In this locality ( $41^{\circ}51'00.3''N$ ;



Fig. 9. Field photograph of a polished fault plane along the Krupnik Fault bringing in contact amphibolite and unconsolidated slope material. Scale is shown by the hammer. Average Plane attitude is 291/62 (dip direction, dip angle). Coordinates of locality is 41°51'46.3"N, 23°10'07.0"E. Altitude 568 m. Photograph location is shown in Fig. 6.

23°08' 58.3"E, 319 m elevation) there is a normal fault down-thrown to the north whose cumulative scarp height exceeds 20 m (Fig. 10). The fault plane disappears beneath the Struma River and its position further west may be inferred by an abrupt change in topographic slope (Fig. 5). Geophysical data (Shanov et al., 1999) from vertical electric soundings also suggest a subsurface dislocation beneath the plain which may be due to a possible displacement of about 3.6 m. Rangelov et al. (2001) also suggest 3–4 m co-seismic displacement during the earthquake. Therefore, we suggest that this fault may have hosted the seismic rupture. The rupture may have crossed the Struma alluvial plain (Fig. 6) with a general E–W strike, a northward dip and with a dip-slip averaging 2 m in alluvium. According to local reports the flow of the Struma River was blocked for several months following the earthquake. We measured the strike and dip of the fault plane using a CLAR compass; the mean attitude is 351/76 (dip direction, dip angle; Fig. 10). The fault also controls local drainage because a small, perennial stream flows along the fault plane until it meets the Struma River. The footwall comprises granite porphyry and amphibolites while the hanging wall consists of sands and clays of Late (?) Quaternary age. The hanging wall is cut by numerous small landslides almost all at right angles to the fault plane indicating unstable ground conditions (Fig. 10). At these localities no striations were measured, however, a NW–SE stress field has been proposed by Shanov and Dobrev (2000) by applying fault slip inversion methods. We note that a 2 m co-seismic displacement has been proposed by Meyer et al. (2002) from field observations along the pre-rift/syn-rift contact, to the east of Krupnik.

#### 4. Structural data and kinematic analysis

We collected field measurements for the orientations of fault-planes, frictional-wear striae on fault planes, and corrugations of fault planes from 15 localities (e.g., Fig. 3). We measured the strike and dip of the fault plane associated



Fig. 10. Field photograph of the 1904 rupture (indicated in Fig. 6). Large, light gray surface is the Krupnik fault scarp. Small cuts at right angles are active landslides. View is to the southeast.

with each striation and corrugation. We measured both the strike and dip of such fault surfaces with a hand-held, CLAR type compass to within  $5^\circ$  total error. Then we measured the rake of the striations and corrugations, using the same hand-held compass. Again, we measured the rake to within about  $5^\circ$  total error.

Three localities represent data from fault planes along the Krupnik fault segment. Three localities show data from the Elovitsa fault. Two localities are located along the Bela fault (point N8 in Fig. 3). One locality is from the Bania fault. One locality is from a fault plane along the Gradevo fault. Another locality is from a fault plane in the footwall of Gradevo fault. Two localities are on the footwall of the Krupnik fault along the provincial road to the town of Brezhani. One locality is a fault plane cross-cutting the Oligocene coal basin near Brezhani (point N15 in Fig. 3).

We analysed all fault-slip data for stress axes orientation using the FAULT software for Windows (Caputo and Caputo, 1988). Selected fault plane orientation data are presented in equal-area, lower hemisphere stereographic projection (Fig. 11). The  $\sigma_1$  axes are represented by triangles, the  $\sigma_2$  are represented by rhombs, and the  $\sigma_3$  are represented by squares. To determine the present-day stress field two methods were applied: the right dihedral (Angelier and Mechler, 1977) and the conditioned square minima (Caputo and Caputo, 1988). Both methods assume that fault motion occurs along the maximum resolved shear stress direction. The slip vector analysis along both the Elovitsa and Bela fault planes shows an N–S tensional stress field (stations N6 and N8; Fig. 3). The older stress regime is directed NE–SW as it was measured by inverting fault slip data from the Brezhani coal basin (station N15 and Fig. 3).

## 5. Coulomb stress modeling

We computed static stress changes due to simple, planar slip along two source faults using the DLC code by R. Simpson (USGS). Modeling parameters are summarized in Table 4. The fault-slip models are based on our field data. The Gradevo segment is 12 km long, strikes  $N210^\circ E$  and dips  $60^\circ NW$ . The rake of the slip-vector was modeled as  $-128^\circ$  (i.e. right-lateral component) in order to comply with the orientation of  $\sigma_3$ . The Elovitsa segment is 11 km long, strikes  $N275^\circ E$  and dips  $60^\circ N$ . The rake of the slip vector was modeled as  $-85^\circ$  (i.e. left-lateral component) in order to comply again with the orientation of  $\sigma_3$ . The two possible source faults for the first 4-4-1904 event share similar fault length ( $L$ ) and width ( $W$ ) values of 12 and 11 km, respectively, so they are capable of producing an earthquake

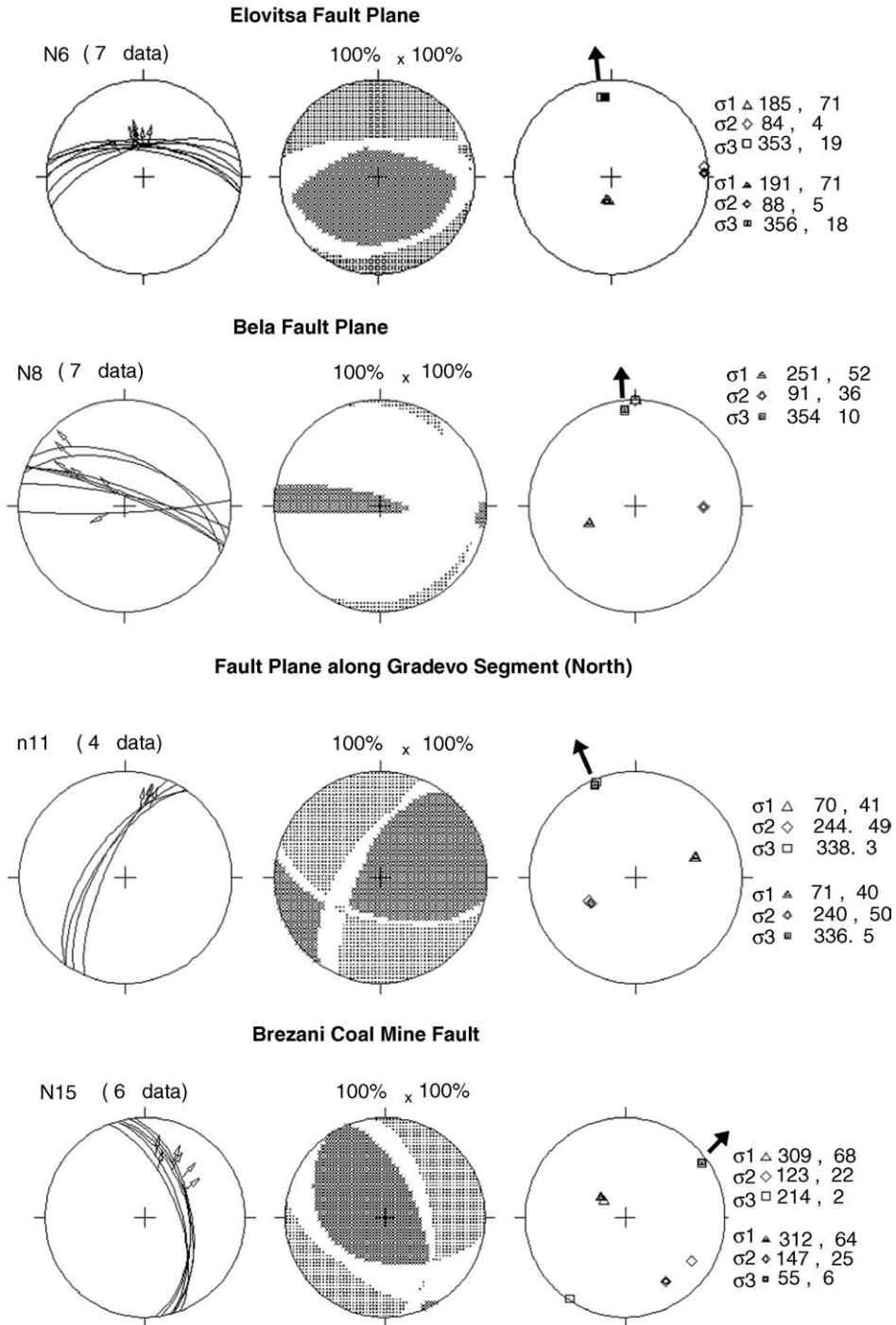


Fig. 11. Stress analysis results:  $\sigma_1, \sigma_2, \sigma_3$  indicate maximum, intermediate and least principal stresses. The  $\sigma_1$  axes are represented by triangles, the  $\sigma_2$  are represented by rhombs, and the  $\sigma_3$  are represented by squares. Numbers after stress symbols indicate azimuth and dip of stress axis. Drawing of the great circles of fault planes (left), areas of the right dihedral method (centre) and principal axes of the stress ellipsoid from the CSM method (right). Arrows on great circles indicate slip directions. Compressional quadrant is dark gray, extensional quadrant as light gray, respectively.

Table 3

Empirical relationships for calculating earthquake magnitude on the basis of geological data (surface rupture length—SRL, co-seismic displacement—D)

Normal	Length (km) vs. magnitude	km	WC	AJ	PC
Ambraseys and Jackson (1998)	$M_s = 5.13 + 1.14 \times \log(L)$	12	6.3	6.3	6.4
Wells and Coppersmith (1994)	$M_w = 4.86 + 1.32 \times \log(\text{SRL})$	20	6.6	6.6	6.7
Pavlidis and Caputo (2004)	$M_s = 0.9 \times \log(\text{SRL}) + 5.48$	36	6.9	6.9	6.9
	Vertical displacement (m) vs. magnitude	$m$	WC	PC	
Wells and Coppersmith (1994)	$M_w = 6.81 + 0.78 \times \log(D)$	2	7.0	6.9	
Pavlidis and Caputo (2004)	$M_s = 0.59 \times \log(D) + 6.75$	3.6	7.2	7.1	

$M_w$  and  $M_s$  indicate moment magnitude and surface magnitude, respectively. The 2 m displacement was obtained by Meyer et al. (2002), while 3.6 m was obtained by Shanov et al. (1999).

of magnitude 6.3–6.4 according to Pavlidis and Caputo (2004; Table 2). Both sources were modeled as inclined, rectangular dislocations ignoring local fault complexities. An isotropic elastic half-space is assumed to represent crustal rheology. We calculated the change in the Coulomb Failure Function (CFF) on both optimal failure planes and along known fault orientations by calculating the static stress change as follows (e.g., Reasenber and Simpson, 1992):

$$\Delta\text{CFF} = \Delta\tau + \mu' \Delta\sigma_n \quad (1)$$

where  $\Delta\tau$  is the co-seismic change in shear stress in the receiver fault and in the direction of fault-slip,  $\Delta\sigma_n$  the change in normal stress (with tension positive), and  $\mu'$  is the effective coefficient of friction, accounting for pore-fluid pressure effects. The CFF function is based on the Coulomb criterion for shear failure of brittle materials. The change of shear stress is computed in the direction of fault slip. Following Stein et al. (1992) and after some algebra:

$$\mu' = \mu(1 - \Delta P/\Delta\sigma_n) \quad (2)$$

where  $\mu$  is the static coefficient of friction and  $\Delta P$  is the pore pressure change within the fault.

The change in the CFF ( $\Delta\text{CFF}$ ) was calculated on a horizontal section at 8 km depth on a 100 km  $\times$  100 km grid surrounding the 10:02 a.m. earthquake epicentre, with 1 km grid spacing, as follows: first, we use the program ELFGRID to calculate a stress tensor grid at 8 km depth. Then we apply the program STROP which uses that tensor to calculate the tractions at that depth on planes of specified strike, dip, and rake. STROP outputs a  $\Delta\text{CFF}$  file that does the calculation in Eq. (1) above on the planes of interest for the friction value specified. Fig. 12 shows the  $\Delta\text{CFF}$  changes on planes having the same geometry (strike N263°E, dip 60°N) and faulting mechanism of the Krupnik (receiver) normal fault. The spatial distribution of the Coulomb stress field has a lobe pattern which is symmetric with respect to the source fault rupture (Fig. 12). We interpret a positive value of  $\Delta\text{CFF}$  to mean that a fault plane occurring within this lobe to have been brought closer to failure; when  $\Delta\text{CFF}$  is negative, the fault is brought further from failure. The final stress field is the sum of the regional stress field and the stress changes generated by our model of the earthquake. A value 0.4 of the effective coefficient of friction was adopted that is closer to friction values for major faults (Harris and Simpson, 1998).

Regarding the Gradevo fault scenario we found that the 10:02 mainshock induced up to 6 bar (0.6 MPa) of positive Coulomb stress change in the immediate region on either side of the source fault, i.e. to the southwest and to the northeast of the hypocentre (Fig. 12a). In addition, almost 2/3 of the Krupnik fault to the west of point B

Table 4

Input parameters used for stress transfer modeling

Poisson ratio	0.25
Shear modulus	$\mu = 300.000$ bar
Projection	UTM zone 34
Hypocentral depth	10 km
Friction coefficient	0.4
Source fault earthquake magnitude	6.3
Rupture length/width—Gradevo scenario	12/10 km
Rupture length/width—Elovitsa scenario	11/10 km

(Fig. 6) is loaded with extra stress of at least 0.86 bar. However, the BD part of the Krupnik segment (Fig. 6) was unloaded up to at least 6 bar as it is located in the footwall area of the Gradevo fault (Fig. 3). This geometry supports the hypothesis that the epicentre of 10:28 a.m. event may have been near the village of Krupnik (Fig. 5) or further west because it is this area of the fault plane that was brought closer to failure. A similar amount of added stress (0.07–6 bar) was calculated for the Krupnik fault in the case of the Elovitsa scenario (Fig. 12b). The new configuration results in a differently oriented  $\Delta$ CFF lobe pattern due to the different strike of the source fault. In both scenarios the maximum distance of the zero-stress contour from the fault tip does not exceed 30 km. Other studies on stress transfer (e.g., Stein et al., 1992; Harris, 1998) have indicated that similar ( $\Delta$ CFF) levels are associated with earthquake triggering on neighbouring faults. Therefore, we cannot conclude in supporting either the Gradevo fault scenario or the Elovitsa fault scenario. Perhaps the Elovitsa scenario is favored by the static stress lobe orientations because the whole length of the target (Krupnik) fault is included within the western positive lobe (compare Fig. 12a and b). In addition, both scenarios predict an increase in stress levels (Fig. 12; more than 0.26 bar) along the normal faults near the town of Razlog (Fig. 4). This amount of extra stress may have advanced the timing of the 1964 event on that area.

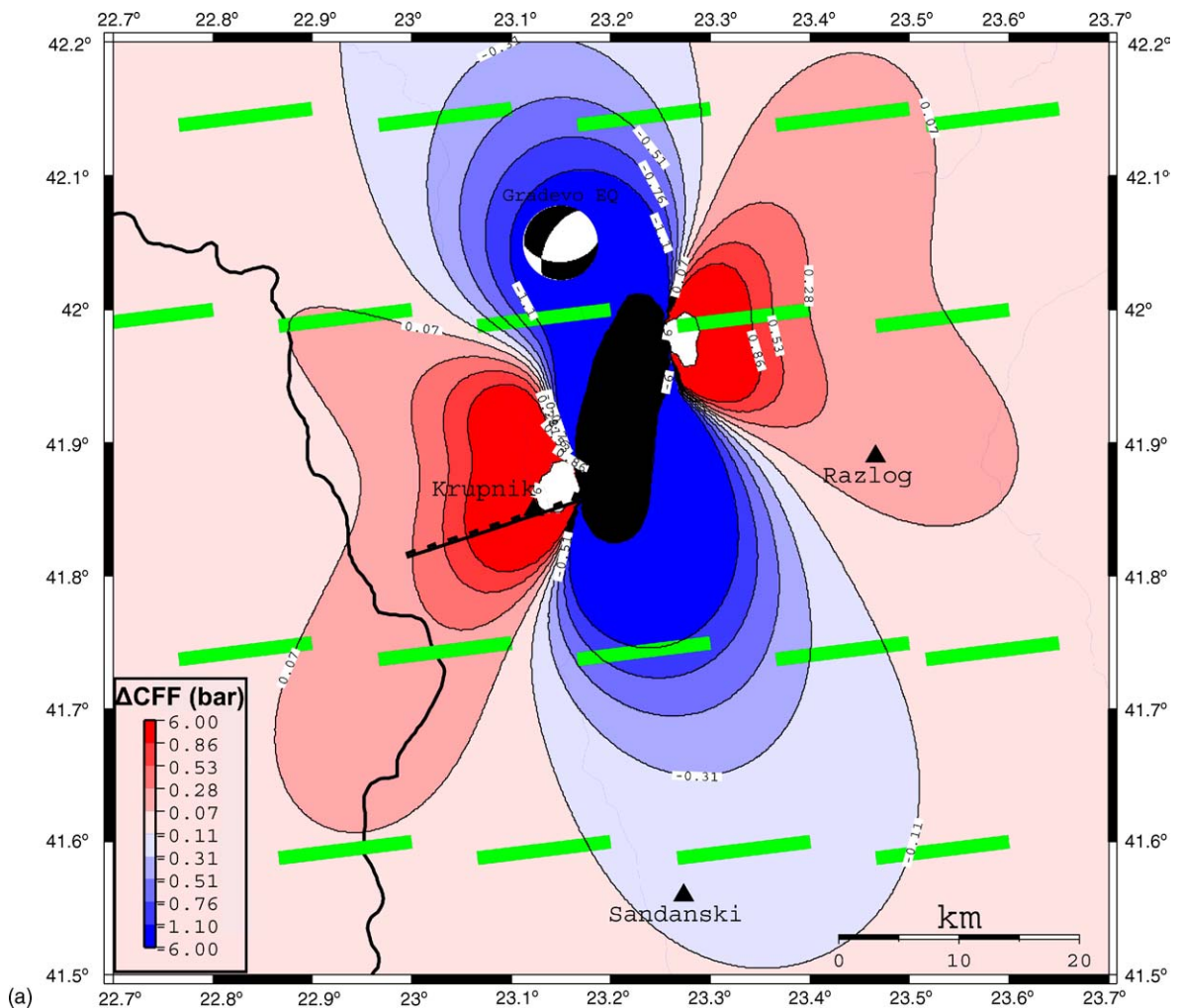


Fig. 12. Maps of co-seismic Coulomb stress changes showing how the 1904 earthquake sequence fits the model of triggered seismicity. Red indicates positive stress change, blue the opposite. The coefficient of friction is 0.4. (a)  $\Delta$ CFF calculation on Krupnik-type receiver normal fault planes assuming rupture along the Gradevo fault. Receiver faults are indicated by green rectangles. For modeling parameters see Table 3. (b)  $\Delta$ CFF calculation on Krupnik-type normal fault planes assuming rupture along the Elovitsa fault.

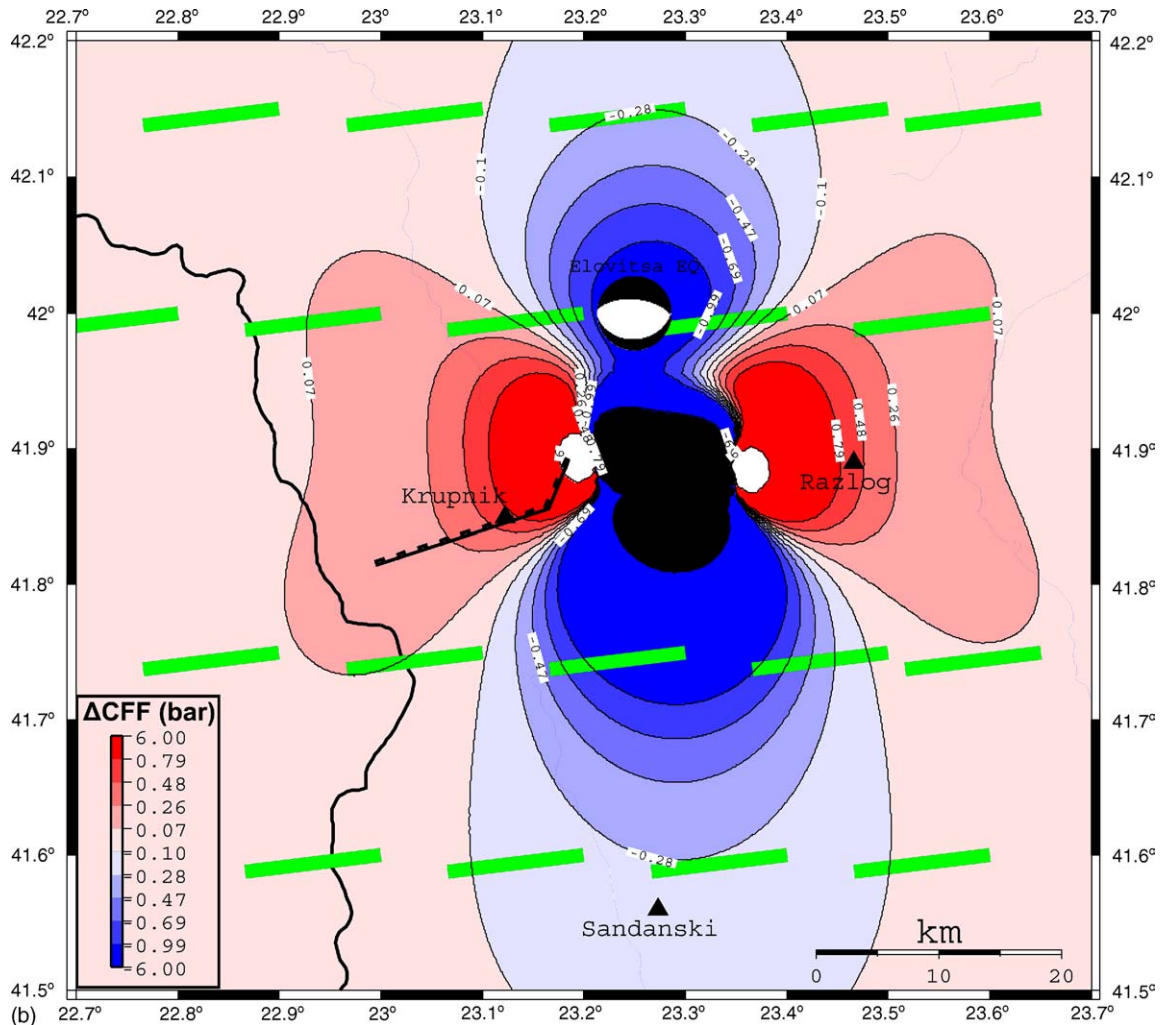


Fig. 12. (Continued).

## 6. Discussion–conclusions

Our field investigations offered the possibility to make a new interpretation for the processes related to the 1904 earthquake sequence. There are two rupture scenarios that may be applicable. First, that the 10:02 event broke the Gradevo and Krupnik segments together. Such a combination of seismic motion would generate a total rupture length of 32–36 km and an earthquake magnitude of  $6.9 \pm 0.3$  (Table 3). The 10:28 event may have occurred further west, inside FYROM. Secondly, the 1904 earthquakes have ruptured two fault segments in southwest Bulgaria (Fig. 3). Without dismissing the 1904 field reports by Hoernes (1904) where large scarps, opened cracks and deep fissures were described to occur to the west of Krupnik, inside the FYROM territory, we support the 2-segment scenario with a total rupture length of 32 km (combined length of Gradevo or Elovitsa and Krupnik segments). According to our static triggering scenario (Fig. 12) the  $M_w$  6.7 earthquake of the 4 April, 1904, 10:25 a.m. occurred along the Krupnik fault segment and it was triggered by the 10:02 a.m.  $M_w$  6.3 event which occurred along either the Gradevo fault or the Elovitsa fault (Fig. 12). On the other hand, it is clear that the ground effects described by Hoernes (1904) need to be investigated by detailed field mapping in order to discriminate between primary seismic rupturing and gravitational sliding and opening due to strong aftershocks.

We also present a set of methods to map the fault segmentation pattern in SW Bulgaria. Our investigation shows that no active fault segment in this region is longer than 20 km. If we accept the second hypothesis that is no single

earthquake event ruptures more than one fault segment, then, by using empirical relationships from geological data on fault rupture length none of the mapped fault segments can accommodate seismic events larger than about  $6.7 \pm 0.3$  (Table 3). Our earthquake magnitude estimates for the 10:02 a.m. event ( $M_w = 6.3$ ) combined with the fault size of approximately  $12 (11) \times 10$  km (length, width; Table 2) yield co-seismic, dip-slip displacements on the hypocentre between 0.43 m (Gradevo fault) and 0.85 m (Elovitsa fault). This result is obtained after applying the Kanamori (1977) formula  $M_w = 2/3 \log M_o - 10.73$ . Such a displacement may have been reduced to about 10–20 cm at ground level (Table 3). On the other hand, the 2 m slip for the co-seismic displacement of the 10:28 a.m. event near the locality shown in Fig. 10 can be used in estimating the earthquake magnitude from empirical magnitude–displacement relationships (Table 3). This way we obtain values between  $M_s$  6.9 and 7.0 which can be regarded as the upper bounds.

Our slip-rate estimate for the Krupnik Fault implies a horizontal extension rate across Krupnik of 0.22 mm/a. In this area a proposed crustal boundary exists (Kotzev et al., 2001) across which a 4 mm/a NW–SE, horizontal extension is estimated. This extension rate requires existence of 18 Krupnik-type faults of which we were able to confirm only 8 (Fig. 4) by field mapping. It is possible that a few more E–W striking, active faults exist along the rift axis Krupnik–Razlog. For example, Dobrev (1999) has mapped normal faults near Simitli that have an antithetic sense of displacement with respect to the Krupnik fault. Other active faults may also exist and need to be confirmed by further field work. The missing faults are situated near the rift axis as the GPS data (Kotzev et al., 2001) suggest that the area to the south of the Krupnik–Razlog Rift moves to the south as a block with an average velocity of  $4 \pm 1$  mm/a. This velocity was measured by the GPS stations southeast of Razlog (DOBR, SAT1; Fig. 1).

Our findings are summarized as follows:

1. We mapped five active fault segments of normal-slip kinematics downthrown to the north. Fault segments are the Krupnik, Gradevo, Elovitsa, Predela and Dobrinishte faults. Along the Predela fault activity has ceased along its northwestern part and all motion is taken by the Elovitsa segment. Three smaller antithetic faults occur near the town of Razlog. These faults are also extensional, normal faults and have been more active during Quaternary than the Predela fault. All fault characteristics are presented in Table 2. The active fault pattern is shown in Figs. 3 and 4. Further work is necessary to map strain patterns in detail along all these faults because of the dense vegetation cover.
2. The 1904 earthquake sequence may have comprised two events that occurred within 20 min of each other and with 10 km distance between them. This two-segment scenario gains support from stress transfer modeling (Fig. 12).
3. The Krupnik fault segment has a general NE–SW strike and dip to the N–NW. Its surface rupture length is about 20 km so its earthquake potential may not exceed a moment magnitude of 6.7 (Table 3). However, according to Pavlides and Caputo (2004) a 20 km fault could produce extreme values of magnitude ( $M_s$ ) ranging between 6.2 and 7.1. Therefore, we note that our result with respect to the magnitude of 10:28 a.m. event, mostly underlines the necessity of more intense investigation in the region. Previous investigations (Rangelov et al., 2000) already underline the ‘existence’ of different magnitude calculations for the 1904 events.
4. A model of Late Tertiary–Quaternary deformation in SW Bulgaria involves a general north–south extension (Fig. 1; Ritsema, 1974; Van Eck and Stoyanov, 1996; Matova et al., 1996; Kotzev et al., 2001). Our study confirms this model and shows that the large, active normal faults are down-thrown to the North. Inversion of fault slip data shows a  $\sigma_3$  axis direction between  $N336^\circ$  and  $N356^\circ$ . Cumulative footwall uplift along the major faults has resulted in the exhumation of the both Pirin and Rila granitoids and the built-up of high topography. This kinematic pattern is clearly a continuation of Aegean-type tectonics into the interior of the Balkan Peninsula.

## Acknowledgements

The authors are greatly indebted to all who assisted in the implementation and completion of this study by providing information, advice and facilities. The mission to SW Bulgaria was conducted during June 2004 and it was financed by the COST Project of the EU (European Cooperation in the field of Scientific and Technical Research; Action 625 “Monitoring of Active Structures”). The Landsat scene was acquired from NASA free of charge. Sotiris Valkaniotis drew Fig. 2. We thank Clark Burchfiel and two anonymous reviewers for constructive reviews. We also thank Bob Simpson, Riccardo Caputo, Efthimios Sokos, Anastasia Kiratzi and Vassilis Karastathis for discussions and George

Stavarakakis for his support. This work is supported by the Bulgarian Ministry of Education and Science and by the General Secretariat for Research and Technology of Greece.

## References

- Allen, P.A., Densmore, A.L., 2000. Sediment flux from an uplifting fault block. *Basin Res.* 12, 367–380.
- Ambraseys, N.N., 2001. The Kresna earthquake of 1904 in Bulgaria. *Ann. Geofis.* 44 (1), 95–117.
- Ambraseys, N.N., Jackson, J.A., 1998. Faulting associated with historical and recent earthquakes in the Eastern Mediterranean region. *Geophys. J. Int.* 133 (2), 390–406.
- Angelier, J., Mechler, P., 1977. Sur une méthode graphique de recherche des contraintes principales également utilisable en tectonique et en séismologie: la méthode des dièdres droits. *Bull. Soc. Geol. France* 19, 1309–1318.
- Caputo, M., Caputo, R., 1988. Structural analysis: new analytical approach and applications. *Ann. Tectonic.* 2, 84–89.
- Christoskov, L., Grigorova, E., 1900. Energetic and space-time characteristics of the destructive earthquakes in Bulgaria after. *Geophys. Inst. Rev.* 12, 79–107 (in Bulgarian).
- Crone, A.J., Haller, K.M., 1991. Segmentation and the co-seismic behavior of basin and range normal faults—examples from east-central Idaho and southwestern Montana, USA. *J. Struct. Geol.* 13 (2), 151–164.
- Dineva, S., Sokerova, D., Michailov, D., 1998. Seismicity of southwestern Bulgaria and border regions. *J. Geodynam.* 26 (2–4), 309–325.
- Dineva, S., Batllo, J., Mihaylov, D., van Eck, T., 2002. Source parameters of four strong earthquakes in Bulgaria and Portugal at the beginning of the 20th century. *J. Seismol.* 6 (1), 99–123.
- Dobrev, N., 1999. Geological hazard processes in the Simitli graben. Ph.D. Thesis, 181 pp. (in Bulgarian).
- Dobrev, N., Kostak, B., 2000. Monitoring tectonic movements in the Simitli Graben, SW Bulgaria. *Eng. Geol.* 57, 179–192.
- Dobrev, N., Frangov, G., Drakatos, G., 2004. Monitoring of active faults along the Strouma Fault Zone, SW Bulgaria. In: *Proceedings of the Fifth International Symposium on Eastern Mediterranean Geology II*, Thessaloniki, Greece, 14–20 April, 2004, pp. 687–690.
- Ganas, A., White, K., 1996. Neotectonic Fault Segments and Footwall Geomorphology in Eastern Central Greece from Landsat TM data. *Geological Society of Greece Special Publication* 6, Athens, pp. 169–175.
- Ganas, A., Papadopoulos, G., Pavlides, S.B., 2001. The 7th September 1999 Athens 5.9  $M_s$  earthquake: remote sensing and digital elevation model inputs towards identifying the seismic fault. *Int. J. Rem. Sens.* 22, 191–196.
- Ganas, A., 2002. Methods for imaging earthquake deformation using satellite data and digital elevation models. In: Gorur, N., et al. (Eds.), *Integration of Earth Science Research on the Turkish and Greek 1999 Earthquakes*. Kluwer Academic Publishers, pp. 197–204.
- Ganas, A., Pavlides, S.B., Sboras, S., Valkaniotis, S., Papaioannou, S., Alexandris, G.A., Plessa, A., Papadopoulos, G.A., 2004. Active fault geometry and kinematics in parnitha mountain, Attica, Greece. *J. Struct. Geol.* 26, 2103–2118.
- Grigorova, E., Sokerova, D., Stoyanov, S., Tzankov, Tz., 1966. Seismo-tectonic characteristics of Razlog earthquake (July 4, 1964). *Bull. Geol. Inst.* 15, 289–311 (in Bulgarian).
- Gutenberg, B., Richter, C.F., 1954. *Seismicity of the Earth and Associated Phenomena*, 2nd ed. Princeton University Press, Princeton, NJ.
- Harris, R.A., 1998. Introduction to special section: stress triggers, stress shadows, and implications for seismic hazard. *J. Geophys. Res.* 103, 24347–24358.
- Harris, R.A., Simpson, R.W., 1998. Suppression of large earthquakes by stress shadows: a comparison of Coulomb and rate-and-state failure. *J. Geophys. Res.* 103, 24439–24451.
- Hoernes, R., 1904. Makedonische erdbeben vom 4. April Mitteilungen der Erdbeben—Kommission der Kaiserlichen, vol. XXIV. Akademie der Wissenschaften in Wien, Neue Folge, Wien.
- Kanamori, H., 1977. Energy-release in great earthquakes. *J. Geophys. Res.* 82 (20), 2981–2987.
- King, G.C.P., Stein, R.S., Lin, J., 1994. Static stress changes and the triggering of earthquakes. *Bull. Seismol. Soc. Am.* 84, 935–953.
- Kotzev, V., Nakov, R., Burchfiel, B.C., King, R., Reilinger, R., 1998. GPS study of active tectonics in Bulgaria: results from 1996 to 1998. *J. Geodynam.* 31 (2), 189–200.
- Marinova, R., Zagorchev, I., 1993. Geological Map of Bulgaria M 1:100,000, Map “Razlog” (in Bulgarian).
- Matova, M., Spiridonov, H., Rangelov, B., Petrov, P., 1996. Major active faults in Bulgaria. *J. Earthquake Predict. Res.* 5, 436–439.
- Meyer, B., Armijo, R., Dimitrov, D., 2002. Active faulting in SW Bulgaria: possible surface rupture of the 1904 Struma earthquakes. *Geophys. J. Int.* 148 (2), 246–255.
- Pavlides, S., Caputo, R., 2004. Magnitude versus faults’ surface parameters: quantitative relationships from the Aegean region. *Tectonophysics* 380 (3/4), 159–188.
- Rangelov, B., van Eck, T., Papadopoulos, G., Pavlides, S., Shanov, S., Schenk, V., 2000. Initial data for the magnitude reevaluation of the strong earthquakes during 1904 in Kresna–Krupnik zone (SW Bulgaria). *Rep. Geodesy Warsaw Univ. Technol.* 4 (49), 51–55.
- Rangelov, B., Rizhikova, S., Toteva, T., 2001. The Earthquake (M7.8) Source Zone (Southwest Bulgaria). Professor Marin Drinov Publishing House, Sofia, p. 279.
- Rangelov, B., Paskaleva, I., 1998. Strong ground motion reconstruction for the earthquakes ( $M=7.8$  and  $M=7.2$ ) in Kresna on 4th April 1904. *Book of Papers, XXVI Gen. Ass. ESC*, Tel Aviv, pp. 231–235.
- Reasenber, P.A., Simpson, R.W., 1992. Response of regional seismicity to the static stress change produced by the Loma Prieta earthquake. *Science* 255, 1687–1690.
- Ritsema, A.R., 1974. The earthquake mechanism of the Balkan region. Royal Netherlands Meteorological Institute, De Bilt, Sct. Report, 74-4, pp. 1–36.

- Roberts, G.P., Koukouvelas, I., 1996. Structural and seismological segmentation of the Gulf of Corinth Fault System: implications for models of fault growth. *Ann. Geofis.* 39 (3), 619–646.
- Shanov, S., Dobrev, N., 2000. Tectonic stress field in the epicentral area of 04.04.1904 Krupnik earthquake from striae on slickensides. *Rep. Geodesy, Warsaw Univ. Technol.* 4 (49), 117–122.
- Shanov, S., Boykova, A., Stoev, D., 1999. Geophysical model of the co-seismic rupturing from the April 4-th 1904 Krupnik Earthquake ( $M=7.8$ , SW Bulgaria). In: *Proceedings of the Second Balkan Geophysical Congress and Exhibition, Istanbul, Turkey, July 5–9, 1999*, pp. 232–233, Book of Abstracts (extended abstract).
- Shebalin, N.V., Karnik, V., Hadzievski, D., 1974. Catalogue of earthquakes, Balkan region. In: *UNDP/UNESCO Survey Seism. Balkan Reg, Skopje*.
- Stein, R.S., King, G.C.P., Lin, J., 1992. Change in failure stress on the Southern San Andreas Fault System caused by the 1992 magnitude = 7.4 Landers earthquake. *Science* 258, 1328–1332.
- Tsapanos, T.M., Vlachos, S.D., Georganta, H.Ch., 2002. The seismic potential assessment for some seismogenic sources in the central northern Greece and its adjacent areas based on the maximum credible magnitude. *J. Balkan Geophys. Soc.* 5 (4), 123–130.
- Van Eck, T., Stoyanov, T., 1996. Seismotectonics and seismic hazard modeling for Southern Bulgaria. *Tectonophysics* 262 (1–4), 77–100.
- Vatzev, M., 1984. Lithostratigraphy of the Paleogene sediments in the Brezhani graben. In: *Zagorchev, I., Mankov, S., Bozhkov, I. (Eds.), Problems of the Geology of SW Bulgaria*. Sofia, Technica, Bulgarian, pp. 36–43.
- Wallace, R.E., 1978. Geometry and rates of change of fault-generated range fronts, North-Central Nevada. *J. Res. U.S. Geol. Surv.* 6 (5), 637–650.
- Wells, D.L., Coppersmith, K.J., 1994. New empirical relationships among magnitude, rupture length, rupture width, rupture area, and surface displacement. *B. Seismol. Soc. Am.* 84 (4), 974–1002.
- Zagorchev, I.S., 1992. Neotectonic development of the Struma (Kraistid) lineament, southwest Bulgaria and northern Greece. *Geol. Magaz.* 2, 197–222.